Quality Control of Surface Wave Data Estimated from Low Signal-to-Noise Ratio HF Radar Doppler Spectra

YUKIHARU HISAKI

Department of Physics and Earth Sciences, Faculty of Science, University of the Ryukyus, Okinawa, Japan

(Manuscript received 7 July 2008, in final form 14 November 2008)

ABSTRACT

Ocean wave spectra estimated by high-frequency (HF) radar are very sensitive to the noise of Doppler spectra. The method for estimating wave spectra has been improved. This method is a nonlinear inversion and can be applied to a single radar case by combining the energy balance equation and the regularization constraint. A simple method for selecting radar-estimated wave data for various weights of the nonlinear weighted least squares problem and initial guesses of the iterative algorithm is proposed. This method is based on the residuals of the objective function to be minimized and is then applied to observed Doppler spectra. The selected radar-estimated wave heights using the method correlated well with in situ observations, even in conditions of low signal-to-noise ratios of Doppler spectra, low wave heights, and small temporal variations of wave heights. The optimal value of the criterion of the residuals is dependent on the required wave height accuracy and number of selected radar-estimated wave data.

1. Introduction

Monitoring sea surface features such as surface currents and waves is important for ocean research and engineering as well as ship navigation and marine pollution prediction. High-frequency (HF) radar can observe ocean surface currents and waves. The surface current is estimated from the Bragg peak of the Doppler spectrum, which is obtained by processing the backscattered radio wave signals from the sea. The ocean wave directional spectrum is estimated by inverting the integral equation, which is the relation between the Doppler spectrum and the wave directional spectrum.

HF radars are widely used for ocean surface current observations in various countries, groups, and areas (e.g., Cochin et al. 2006; Hisaki and Naruke 2003; Hisaki 2006b; Kohut et al. 2006; Paduan et al. 2006). On the other hand, the observations of ocean wave spectra by HF radars (e.g., Hisaki 2005, 2006a; Wyatt et al. 2003; Lipa and Nyden 2005) have not been as extensive as those of surface currents. One reason is that wave estimation by HF radar is much more complicated than surface current estimation. The other reason is that the radar-estimated wave data are much more sensitive to the noise of the Doppler spectrum than radar-estimated surface currents. Therefore, a method for estimating ocean wave spectra that is robust to noise should be developed. In addition, if the Doppler spectrum is contaminated significantly by the noise and if it is unavoidable that the radar-estimated wave data are eliminated, a method of selecting or eliminating the radar-estimated wave data should be developed.

Hisaki (2005, 2006a) developed a method to estimate ocean wave spectra from HF radar Doppler spectra. This method uses the energy balance equation and regularization constraints in addition to the relationship between the Doppler spectrum and the ocean wave spectrum. These equations are converted to a nonlinear weighted least squares problem, where the objective function to be minimized is the sum of the weighted squared residuals of the equation, as explained in section 2a. As a nonlinear inversion method, this method is different from other methods. Even though the Doppler spectra are missing at a few positions, it is possible to estimate the wave spectra at those points. This method is used for the single radar case, and it is possible to extend the method for a dual radar system.

On the other hand, one disadvantage of this method is that it is computationally difficult because of the large-scale

Corresponding author address: Yukiharu Hisaki, Department of Physics and Earth Sciences, Faculty of Science, University of the Ryukyus, 1 Aza-Senbaru, Nishihara-cho, Nakagami-gun, Okinawa 903-0213, Japan.
E-mail: hisaki@sci.u-ryukyu.ac.jp

DOI: 10.1175/2009JTECHO653.1

nonlinear least squares problem. Another disadvantage is that the solution of the nonlinear least squares problem is dependent on the initial guess for the iterative algorithm to solve the nonlinear least squares problem. A third disadvantage is that the solution is dependent on the weights in the objective function. The second and the third disadvantages are the focus of the present study. Hashimoto et al. (2003) developed a method to determine the weights of the regularization constraint for the dual radar system. However, it is not feasible for the present method because of the large number of unknowns to be estimated.

The radio wave and ocean wave conditions of the analyzed data are not good in the present study; for example, the signal-to-noise ratios (SNRs) of Doppler spectra are low, as described in section 4b. In addition, the wave heights are low, and the temporal variability of waves is low (section 4c). Under these conditions, the quality control of the Doppler spectra and radar-estimated wave data is critical for the accuracy of the wave estimation.

The objectives of the paper are as follows: first, to develop a simple method to control the radar-estimated wave data, even when the SNR Doppler spectra are low, and then to develop a simple method to select radar-estimated wave data from various solutions. The method to estimate ocean wave spectra from HF radar is described in section 2. The methods for processing the Doppler spectra and wave data are described in section 3. The HF radar and in situ observations are described in section 4. Examples of the wave estimation are described in section 5a. The results of the wave selection are given in section 5b. Section 6 discusses the results and future subjects.

2. Method to estimate wave spectrum

a. Formulation

The method is almost same as those of Hisaki (2005, 2006a), which is described in detail therein. The HF radar is the narrow beam type, and Doppler spectra are obtained on polar grid points with the origin at the radar position. Wave spectra are estimated on the grid points of the polar coordinates (r, θ_b), as shown in Fig. 1. The wave spectra $F = F(\omega, \theta) = F(r, \theta_b, \omega, \theta)$ are functions of distances from the radar r, beam directions θ_b, radian wave frequencies ω, and counterclockwise wave directions θ with respect to the eastward orientation. The wave spectral values are estimated for grid points $[r(i_r), \psi(j_b), \omega(k_f), \theta(l_d)]$ in four-dimensional $(r$–θ_b–ω–$\theta)$ space, and

$$r(i_r) = r_{\min} + \Delta_r(i_r - 1), \quad i_r = 1, \ldots, N_r, \tag{1}$$

$$\psi(j_b) = \psi_{\min} + \Delta_\psi(j_b - 1), \quad j_b = 1, \ldots, N_B, \tag{2}$$

$$\omega(k_f) = \omega_{\min}\Delta_\omega^{k_f - 1}, \quad k_f = 1, \ldots, M_f, \quad \text{and} \tag{3}$$

$$\theta(l_d) = -\pi + \frac{2\pi(l_d - 1)}{M_d}, \quad l_d = 1, \ldots, M_d, \tag{4}$$

where $r(i_r)$ is the distance between the radar and the grid point for the range (distance from the radar) index number i_r, $r_{\min}$ is the closest distance from the radar, Δ_r is the range resolution, $\psi(j_b)$ is the beam direction for a beam index number j_b (hereafter the direction is the counterclockwise angle with respect to the eastward direction), $\psi_{\min}$ is the rightmost direction, Δ_ψ is the beam resolution, $\omega(k_f)$ is the wave radian frequency for the frequency index number k_f, $\omega_{\min}$ is the minimum radian frequency, Δ_ω is the frequency increment, $\theta(l_d)$ is the wave direction for the wave direction index number l_d, N_r is the number of ranges, N_B is the number of beams, M_f is the number of wave frequencies, and M_d is the number of wave directions.

The observed data by HF radar is the Doppler spectrum $P(\omega_D)$, where ω_D is the radian Doppler frequency. The Doppler spectrum $P(\omega_D)$ is separated into $P_1(\omega_D)$ and $P_2(\omega_D)$, where $P_m(\omega_D)$ is the first-order $(m = 1)$ and second-order $(m = 2)$ Doppler spectrum, and $P(\omega_D) = P_1(\omega_D) + P_2(\omega_D)$. The first-order Doppler spectrum $P_1(\omega_D)$ is determined by identifying local minima around the two first-order scattering peaks in the Doppler spectrum $P(\omega_D)$. The first- and second-order Doppler spectra $P_m(\omega_D)$ $(m = 1, 2)$ are calibrated as

$$P_{cm}(\omega_D) = P_m(\omega_D)\left[\int_{-\infty}^{+\infty} P_1(\omega_D)\, d\omega_D\right]^{-1}, \quad (m = 1, 2) \tag{5}$$

for wave estimation.

The equations for estimating wave spectra are as follows:

1) The relationship between first-order Doppler spectra and wave spectra is

$$\Phi\left\langle\left\{\int_0^\infty \sigma_1[(2m-3)\omega_D]\, d\omega_D\right\}\left[\int_{-\infty}^{\infty}\sigma_1(\omega_D)\, d\omega_D\right]^{-1}\right\rangle = \Phi\left\{\int_0^\infty P_{c1}[(2m-3)\omega_D]\, d\omega_D\right\}, \quad (m = 1 \text{ or } 2), \tag{6}$$

where $\sigma_1(\omega_D)$ is the first-order radar cross section, which is given in Eq. (A1).

2) The relationship between second-order Doppler spectra and wave spectra is

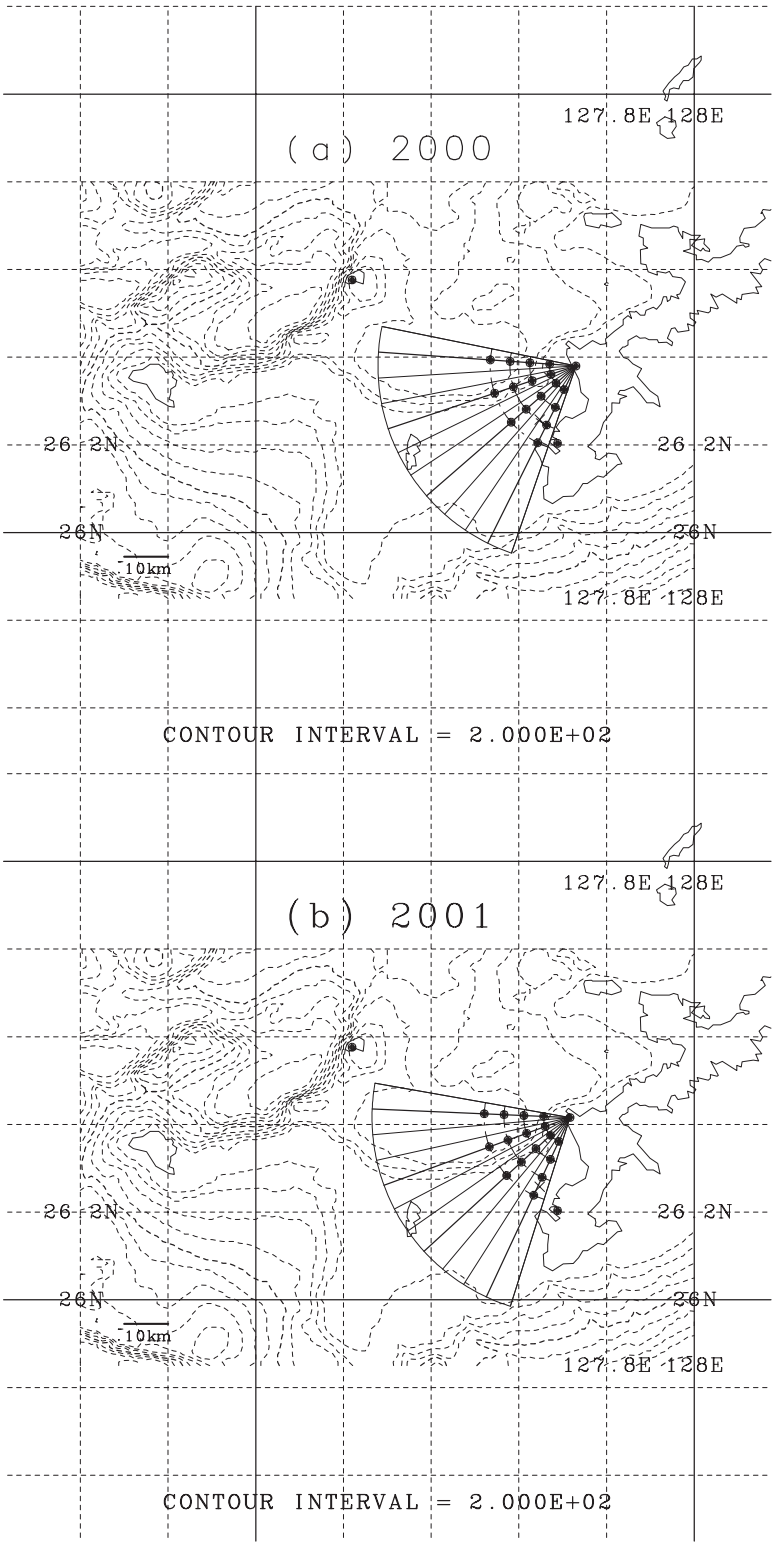

FIG. 1. HF radar observation area for (a) 2000 and (b) 2001. Radar positions (denoted by •), radial grids to estimate wave spectra, and wind station. Wave station at 26.26°N, 127.65°E (USW; denoted by ×).

$$\Phi\left\{\sigma_2(\omega_D)\left[\int_{-\infty}^{\infty}\sigma_1(\omega_D)\,d\omega_D\right]^{-1}\right\} = \Phi[P_{c2}(\omega_D)], \quad (7)$$

where $\sigma_2(\omega_D)$ is the second-order radar cross section, which is given in Eq. (A2). The function Φ is given as $\Phi(\sigma) = \log(\sigma)$ in Hisaki (2005, 2006a).

3) The wave energy balance equation is under the assumption of stationarity [Eq. (A5)].
4) The continuity equation of wind vectors is under the assumption of no horizontal divergence [Eq. (A6)].
5) Regularization constraints are in wave frequency–wave direction grids [Eq. (A7)].
6) Regularization constraints are in spatial radial grids [Eq. (A8)].

The first- and second-order radar cross sections [$\sigma_m(\omega_D)$, $m = 1, 2$] in Eqs. (6) and (7) are written in terms of the wave spectrum $F(\omega, \theta)$ (Barrick 1971a) as Eqs. (A1) and (A2). The Eqs. (7) and (A2) are the nonlinear integral equations, and the discretization of the integral equation is described in Hisaki (1996).

These constraints are called constraints 1–6. The unknowns to be estimated are the wave spectral values and wind vectors. The number of unknowns is $N_u = N_s + 2N_g$, where $N_g = N_r N_B$ is the number of radial grids and $N_s = M_f M_d N_g$ is the number of spectral values. The total number of constraints is

$$\begin{aligned} N_t &= 3N_s + 2N_g + K_{\mathrm{DT}}, \\ &= 3M_f M_d N_r N_B + 2N_r N_B + K_{\mathrm{DT}}, \end{aligned} \quad (8)$$

where K_{DT} is the total number of second-order Doppler spectral values for wave estimation.

The equations from (A1) to (A8) are normalized by the Bragg wavenumber $2k_0$ and the radian Bragg frequency $\omega_B = [2gk_0\tanh(2k_0d)]^{1/2}$, where g is the gravitational acceleration, k_0 is the radio wavenumber, and d is the water depth (Lipa and Barrick 1986).

Even when a few Doppler spectra on the radial grid points are missing, the total number of constraints is larger than the number of unknowns (i.e., $N_t > N_u$). Therefore, it is possible to estimate the wave spectrum at the grid points where the Doppler spectra are missing.

The parameterizations of the source function in the energy balance equation [constraint 3 or Eq. (A5)] are the same as those in the WAMDI group (1988). These equations are discretized in terms of wave spectral values in four-dimensional space and wind vectors on the polar grids.

Thus, we seek the N_u-dimensional vector $\mathbf{x}$ to minimize the objective function defined as the sum of weighted squared differences of constraints 1–6, or

$$U(\mathbf{x}) = \frac{1}{2}\sum_{K=1}^{N_t}[\lambda_{wM}F_K(\mathbf{x})]^2 = \frac{1}{2}\sum_{K=1}^{N_t}[f_K(\mathbf{x})]^2, \quad (9)$$

where the N_u-dimensional vector $\mathbf{x}$ denotes spectral values, wind speeds, and directions and F_K corresponds to constraints 1–6. The parameter λ_{wM} ($M = 1, \ldots, 6$) is the weight for the constraint M [Eqs. (6), (7), and (A5)–(A8)].

b. Algorithm

The process to seek $\mathbf{x}$ to minimize $U(\mathbf{x})$ [Eq. (9)] is divided into three steps. In the first step, the estimated wave spectrum does not depend on the radial grids. The estimated wave spectrum is expressed by the parametric form as Eqs. (B1)–(B5) (Hisaki 2006a), and the parameters are estimated by the Monte Carlo method. The wind direction is also estimated in the first step. The initial wind direction is estimated only from the ratios of first-order scattering, such as in the method described in Hisaki (2002, 2007).

The wave spectrum is also independent of the radial grids in the second step. The $M_f M_d$ spectral values are estimated in the second step from constraints 1 [Eq. (6)], 2 [Eq. (7)], and 5 [Eq. (A7)]. The spectral values estimated in the second step are initial guesses for the third step. The steepest descent method, or Levenberg–Marquardt method, is adopted to seek the $M_f M_d$ spectral values. If the iterative algorithm to seek the $M_f M_d$ spectral values does not converge, the spectral values inferred by the Monte Carlo method as in the first step are initial guesses in the second step. The initial wind speed is empirically estimated from initial spectral values at high frequencies in the second step.

The third step is the iterative algorithm to estimate the N_u-dimensional vector $\mathbf{x}$ (Hisaki 2006a). The number of unknowns N_u is large, more than several thousand. It is impossible to store the $N_u \times N_u$ matrix in the memory of a personal computer. The steepest descent method or a modified form of the steepest descent method is used (Hisaki 2005, 2006a). The updating vector is obtained by multiplying the gradient vector of $U(\mathbf{x})$ [Eq. (9)] by a positive definite diagonal matrix from the left as Eq. (B10). The details of the iterative algorithm for the large number of unknowns are described in Hisaki (2006a). The equations for the algorithm are given in Eqs. (B6)–(B10) in appendix B. The iterative algorithm is stopped by the number of iterations (105).

c. Modifications from previous studies

As explained in section 4b, the SNR of the observed Doppler spectrum is low. Therefore, the methods are

modified in the following points. One modification is that the function $\Phi(\sigma) = \sigma$ in Eqs. (6) and (7), whereas $\Phi(\sigma) = \log(\sigma)$, as given in Hisaki (2005, 2006a).

If the SNR is low and if Doppler spectral values close to the noise level are used for wave estimation, the function $\Phi(\sigma)$ must be a linear function, because the noise level is subtracted from the Doppler spectrum and the wave spectrum is sensitive to small Doppler spectral values in the case of $\Phi(\sigma) = \log(\sigma)$. On the other hand, the radar-estimated wave height is dependent on the largest second-order Doppler spectral values in the case of $\Phi(\sigma) = \sigma$. The radar-estimated wave height in the case of $\Phi(\sigma) = \sigma$ is more sensitive to spurious Doppler signals than that in the case of $\Phi(\sigma) = \log(\sigma)$.

The other modification is that the Doppler frequency range for wave estimation is extended. The Doppler frequency range for wave estimation in Hisaki (2005) is near the second-order Doppler peaks. If the Doppler spectral values only in the four sidebands are used for wave estimation, then the ocean wave spectral values at higher frequencies are often overestimated; the retrieved Doppler spectral values are overestimated at lower or higher Doppler frequencies, where the Doppler spectral values are not used for wave estimation. To avoid this overestimation of the retrieved Doppler spectrum and radar-estimated wave height, the Doppler frequency range for wave estimation is extended. The second-order Doppler spectral values close to zero are used for wave estimation, but the small Doppler spectral values are not sensitive to wave estimation, because the contribution of these values to the objective function $U(\mathbf{x})$ [Eq. (9)] is small in the case of $\Phi(\sigma) = \sigma$. These modifications from Hisaki (2005) are due to the low-SNR Doppler spectra analyzed in this study.

3. Data processing

a. Radar and wave parameters

The radar parameters are as follows: the radiowave frequency of the HF radar is 24.5 MHz, and the radio wavelength is $2\pi/k_0 = 12.2$ m. The Bragg frequency is $f_B = \omega_B/(2\pi) = 0.506$ Hz. The range and beam resolutions of the radar are 1.5 km and 7.5°, respectively. The Doppler spectra are spatially averaged: the 3 (range) × 3 (beam) = 9 Doppler spectra are averaged to reduce the number of unknowns N_u. The range resolution [Eq. (1)] is $\Delta_r = 4.5$ km, and the number of ranges is $N_r = 4$. The beam resolution [Eq. (2)] is $\Delta_\psi = 22.5°$, and the number of beam directions is $N_B = 4$. The number of radial grids is $N_g = 16$.

The Doppler frequency ranges of the second-order scattering for wave estimation are $0 \le |\omega_{\mathrm{DN}}| \le 0.45$ at the 0.15 interval, $0.6 \le |\omega_{\mathrm{DN}}| \le 0.96$ at the 0.04 interval, and $1.04 \le |\omega_{\mathrm{DN}}| \le 1.4$ at the 0.04 interval, where $\omega_{\mathrm{DN}} = \omega_D/\omega_B$ is the normalized Doppler frequency. The values of $P_{c2}(\omega_D)$ [Eq. (7)] within the first-order scattering Doppler frequency ranges, which are between local minima near the Bragg peaks, are replaced with small positive values. The values of $P_{c2}(\omega_D)$ near the zero Doppler frequency are also replaced with small positive values. The radar-estimated wave height is not sensitive to small positive values in the case where $\Phi(\sigma) = \sigma$ [Eq. (7)].

The wave parameters estimated by the HF radar are as follows: the wave frequency parameters in Eq. (3) are $\Delta_\omega = 1.15$, $\omega_{\min}/(2\pi) = 0.049$ Hz, and $M_f = 21$. The maximum wave frequency is $\omega_{\max}/(2\pi) = 0.813$ Hz. The wave direction parameter in Eq. (4) is $M_d = 18$. The number of unknowns is $N_u = N_g M_f M_d + N_g = 6080$.

b. Weights of constraints

The solution $\mathbf{x}$ in Eq. (9) is dependent on the weights λ_{wM} ($M = 1, \ldots, 6$). The solution $\mathbf{x}$ is also dependent on the initial guess in the second step (section 2b), and the initial guess is dependent on the weights λ_{w1} [Eq. (6)], λ_{w2} [Eq. (7)], and λ_{w5} (constraint 5 in section 2a).

The weights $\lambda_{w1} = (\nu_1/\nu_2)^{1/2}$ and $\lambda_{w2} = 1$, where ν_1 and ν_2 are the degrees of freedom of the integrated first-order and the second order Doppler spectra, respectively. Typical values are $\nu_1 = 72$ and $\nu_2 = 11$ (e.g., Hisaki 2005).

The initial guesses in the second step are calculated for the following:

- Case A: $\lambda_{w5} = 10^{-2}$;
- Case B: $\lambda_{w5} = 10^{-1}$; and
- Case C: $\lambda_{w5} = 1$.

The solutions $\mathbf{x}$ in the third step are calculated for the following:

- Case 1: $(\lambda_{w2}, \lambda_{w3}, \lambda_{w5}) = (10^2, 1, 1)$, $\lambda_{w4} = 1$, $\lambda_{w6} = \lambda_{w5}$;
- Case 2: $(\lambda_{w2}, \lambda_{w3}, \lambda_{w5}) = (10^3, 1, 1)$, $\lambda_{w4} = 1$, $\lambda_{w6} = \lambda_{w5}$; and
- Case 3: $(\lambda_{w2}, \lambda_{w3}, \lambda_{w5}) = (10^2, 10, 1)$, $\lambda_{w4} = 1$, $\lambda_{w6} = \lambda_{w5}$.

The wave spectra are estimated for 3 (second step) × 3 (third step) = 9 cases. If the second step is case B and if the third step is case 1, to estimate the solution $\mathbf{x}$, it is referred to as case B-1.

c. Processing of Doppler spectra

The nine Doppler spectra are spatially averaged. Doppler spectra are often affected by spurious signals. It is desirable to remove the Doppler spectra affected by spurious signals from the calculations.

The radar-estimated wave height H_r is approximately proportional to

$$R_{12} = \left[\frac{\int_{-\infty}^{\infty} P_2(\omega_D)/w(\omega_{\mathrm{DN}})\, d\omega_D}{\int_{-\infty}^{\infty} P_1(\omega_D)\, d\omega_D} \right]^{1/2}, \qquad (10)$$

where $w(\omega_{\mathrm{DN}})$ is the weighting function for normalized Doppler frequency $\omega_{\mathrm{DN}} = \omega_D/\omega_B$ defined in Barrick (1977). If R_{12} is much larger than the other R_{12} values of the back and forth time, the Doppler spectrum is excluded from the averaging.

The noise floor is subtracted from the average Doppler spectrum. The noise floor is evaluated by the rank ordering technique (Heron and Heron 2001). The Doppler spectral values P are sorted from the smallest value and plotted as a function of cumulative probability q. The $[-2\log(q)]^{1/2}$ and P plot is drawn. The noise-dominated part of the Doppler spectrum is expressed by the straight line in the $[-2\log(q)]^{1/2}$ and P plot (e.g., Fig. 4 in Heron and Heron 2001). The straight line expressing the noise-dominated part is evaluated by the least squares method, and the noise floor of the Doppler spectrum is estimated.

d. Selection of wave data

The selection of radar-estimated wave data is based on residuals of the objective function [Eq. (9)]. The logarithm of the root of the residual of the second-order radar cross-sectional equation [Eq. (7)] is

$$R_s = \frac{1}{2}\log\left[\frac{1}{K_{\mathrm{DT}}} \sum_{K=N_g+1}^{N_g+K_{\mathrm{DT}}} F_K^2(\mathbf{x}) \right]. \qquad (11)$$

The residual of constraint 3 (energy balance equation) is used; however, instead of the residual of the constraint, the rate of wave height change represented as

$$F(t+\Delta t) = F(t) + (-\mathbf{C}_g \nabla F + S_t)\Delta t, \qquad (12)$$

$$H_r(t) = 4\left[\int_{\omega_{\min}}^{\omega_{\max}} \int_{-\pi}^{\pi} F(\omega, \theta, t)\, d\theta\, d\omega \right]^{1/2}, \quad \text{and} \qquad (13)$$

$$H_{\mathrm{dif}} = |H_r(t+\Delta t) - H_r(t)| \qquad (14)$$

is calculated, where $F = F(t) = F(\omega, \theta, t)$ is the radar-estimated wave spectrum at the time t, $\mathbf{C}_g = (C_g \cos\theta, C_g \sin\theta)$ is the group velocity vector, ∇ denotes the horizontal gradient on the polar coordinate with the origin at the radar position, and S_t is the source function.

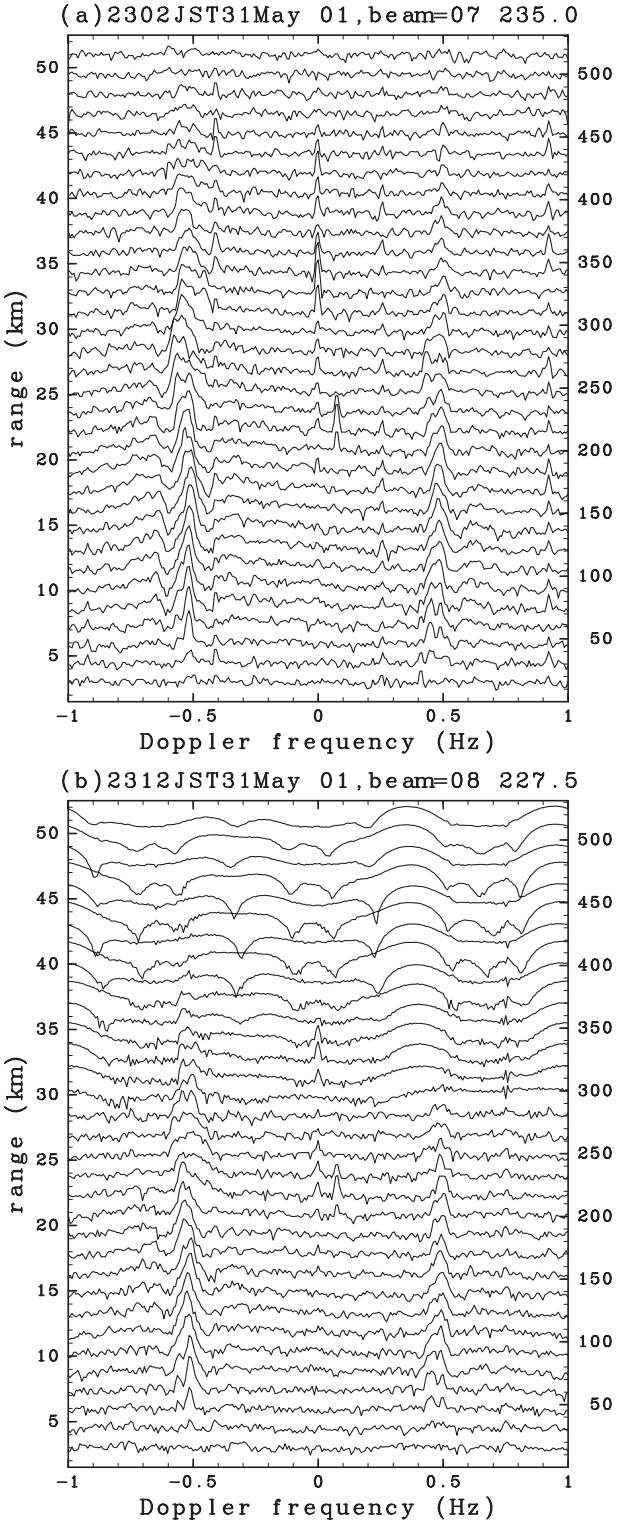

FIG. 2. Examples of Doppler spectra for various ranges (distances from the radar) and the beam directions (a) 235° and (b) 227.5°T. The left vertical axis indicates the distance of each Doppler spectrum from the radar. The right vertical axis indicates the relative signal intensity in decibels.

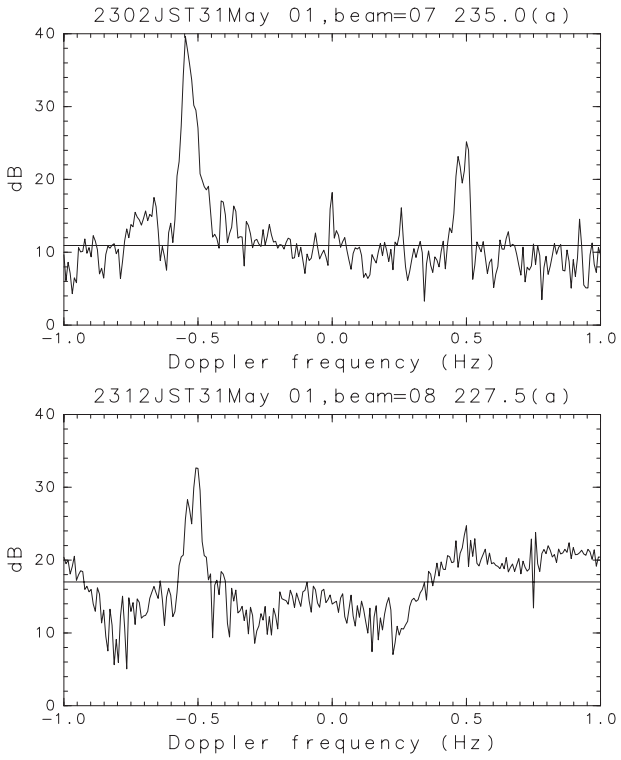

FIG. 3. Examples of Doppler spectra, with solid straight line denoting noise levels estimated by rank ordering technique (Heron and Heron 2001).

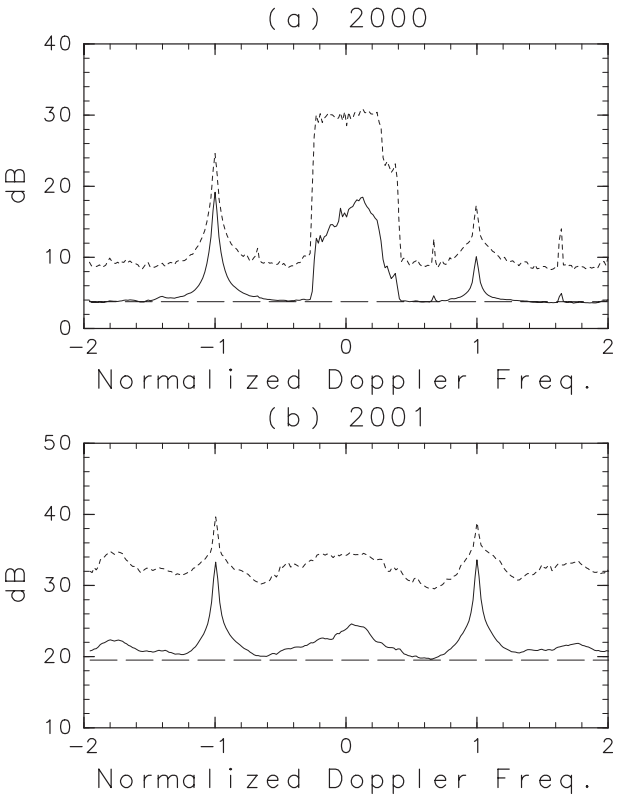

FIG. 4. Averaged noise floor (dashed line), averaged noise floor plus noise-subtracted Doppler spectra (solid line), and averaged noise floor plus std dev (dotted line) for (a) 2000 and (b) 2001.

The time step is $\Delta t = 2$ h here, because the time interval of both the radar and ultrasonic wave gauge (USW) wave height is 2 h. We can calculate $F(t + \Delta t)$ from the radar-estimated wave spectrum $F = F(t) = F(\omega, \theta, t)$ by Eq. (12). The wave heights $H_r(t + \Delta t)$ and $H_r(t)$ are calculated from $F(t + \Delta t)$ and $F(t)$, and H_{dif} is calculated from Eq. (14).

The wave data are selected from nine cases (section 3b) by using the following procedure:

1) Find the minimum R_s.
2) If $R_s < R_{\text{smax}}$ and $H_{\text{dif}} < H_{\text{dmax}}$ and the frequency spectrum decreases as the frequency increases, then the wave data are selected.
3) Otherwise, the wave data are not selected.

This selection is conducted for various values of R_{smax} and H_{dmax}.

4. Observation

a. HF ocean radar and in situ observations

Observation of surface waves was conducted in the west of Okinawa Island in Japan by using the HF ocean radars of the Okinawa Radio Observatory, Communications Research Laboratory (Okinawa Subtropical Environment Remote Sensing Center, National Institute of Information and Communications Technology) from 21 October to 7 December 2000 and from 26 May to 2 July 2001. The observation map is shown in Fig. 1. The HF radar system is the ground wave system, in which the radio wave is guided along the surface of the earth. The Doppler spectra are sampled on polar grid points, with the origin at the radar position. The temporal resolution of the radar system is 2 h. The radar was of the beam-forming type, with the beam forming electronically controlled by a phase shifter in real time. The beam step was 7.5°. The HF ocean radar system is described in Hisaki et al. (2001).

The location of the HF radar was 26.38°N, 127.73°E in 2000 and 26.42°N, 127.72°E in 2001. The beam directions were from 199° to 281.5° from true north (T) in 2000 and from 197.5° to 280°T in 2001. The radar beam in 2000 was directed in a more landward direction than that in 2001, because of the difference of the radar position. The Doppler spectra were spatially averaged, and wave spectra were estimated by the 16 radial grid points in Fig. 1.

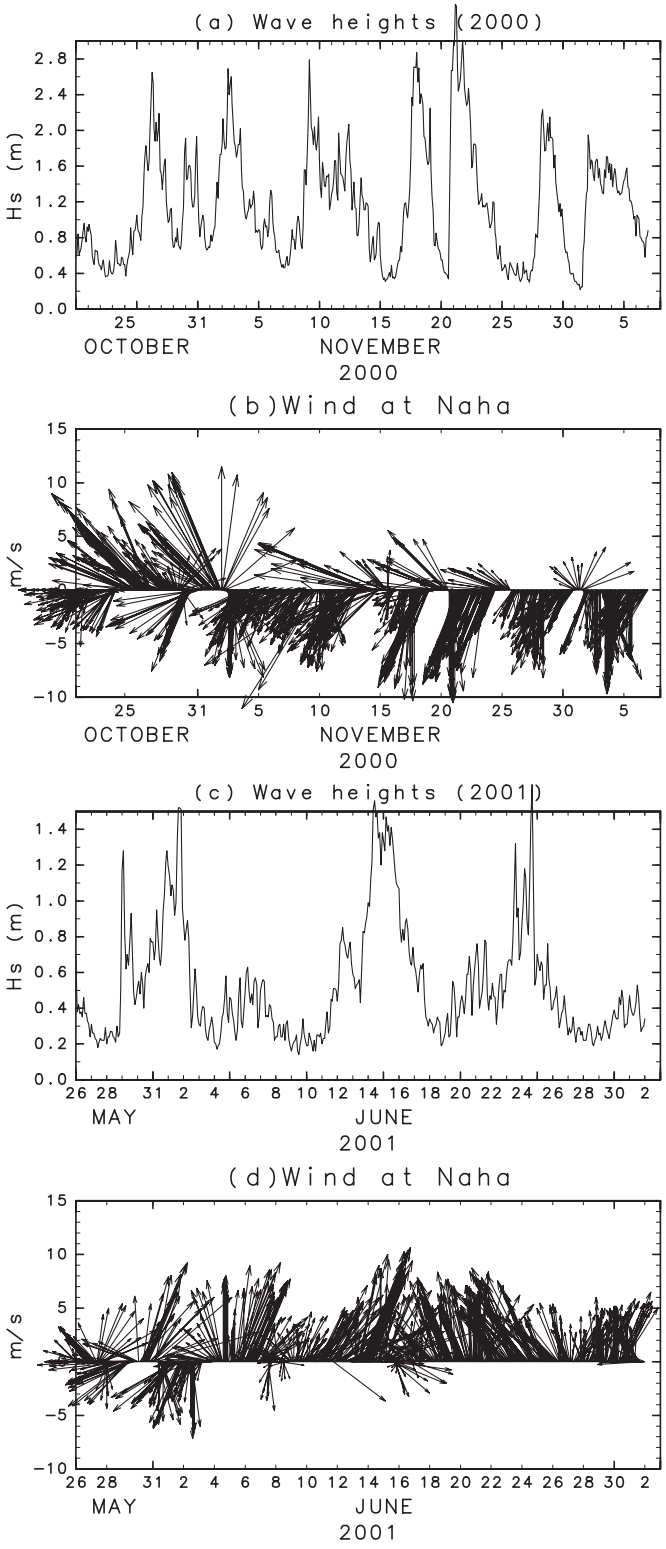

FIG. 5. Time series of (a) significant wave heights H_s and (b) wind vectors in 2000. Time series of (c) significant wave heights H_s and (d) wind vectors in 2001.

The waves were observed by USW at 2-h intervals in 26.26°N, 127.65°E, where the water depth is 53 m. The significant wave heights H_s were estimated by the zero-up-cross method. The closest radial grid point to the USW in Fig. 1 was $(i_r, j_b) = (3, 4)$ in both 2000 and 2001, where i_r and j_b are the range and beam number index, respectively.

The wind speeds and directions are observed at 10-min intervals off of Okinawa Island by the Japan Meteorological Agency (JMA) at 26.20°N, 127.69°E. The resolution of wind speed is 1 m s^{-1}, and the resolution of wind direction is 22.5°.

b. Doppler spectrum

Figure 2 shows examples of Doppler spectra as a function of Doppler frequency $f_D = \omega_D/(2\pi)$. The periodic structures of Doppler spectra can be clearly seen in Fig. 2b at a range greater than the 30-km range. For example, the uppermost Doppler spectrum has gentle peaks at $f_D \simeq 0.35$ Hz and $f_D \simeq 0.95$ Hz in Fig. 2b, which are not first- or second-order Doppler spectrum peaks. These periodic structures show that the Doppler spectra are strongly affected by spurious signals, although the source of the spurious signals is unclear. Figure 2a seems to be better Doppler spectra in the HF radar observation period. Figure 3 is the Doppler spectrum at the range of 30 km in Fig. 2a. The noise floor is also indicated in Fig. 3. The noise floor is estimated by the rank ordering technique (Heron and Heron 2001). The data quality of the Doppler spectrum in Fig. 3a is not as bad in the datasets of the present study. However, the second-order Doppler spectrum peak at $f_D \simeq -0.7$ Hz is larger than the noise floor by only 6 dB. In Fig. 3b, the periodic structure in the Doppler spectrum at the range of 30 km is unclear. But we can see that the Doppler spectrum in Fig. 3b is also affected by the spurious signals.

The mean SNRs during the HF radar observation period and over the analysis area are estimated in the following procedure: noise floors are estimated by the rank ordering technique (Heron and Heron 2001). The noise floors are subtracted from the Doppler spectra. Both noise-subtracted Doppler spectra and noises are averaged in time and space. Averaged noise-subtracted Doppler spectra and noises are summed. All of the Doppler spectra in the analysis area and period are averaged. The effects of the surface currents are corrected. The standard deviations are also estimated.

Figure 4 shows the mean SNRs during the HF radar observation period in 2000 and 2001. The mean noise floor, the mean noise floor plus the mean noise-subtracted Doppler spectra, and the mean noise floor plus the standard deviation of the noise-subtracted Doppler spectra are indicated in Fig. 4. The mean noise-subtracted Doppler spectral values are small, except in the first-order scattering Doppler frequency and the zero Doppler frequency in 2000 (Fig. 4a); this shows that the mean SNR is almost 0 dB. The peaks in Fig. 4a near the zero Doppler frequency are associated with the echoes reflected from the land. The echoes reflected from the land cannot be seen in Fig. 4b, because the beam directions in 2001 are different from those in 2000 (Fig. 1). The standard deviation is about 6 dB. This shows that most of the SNRs

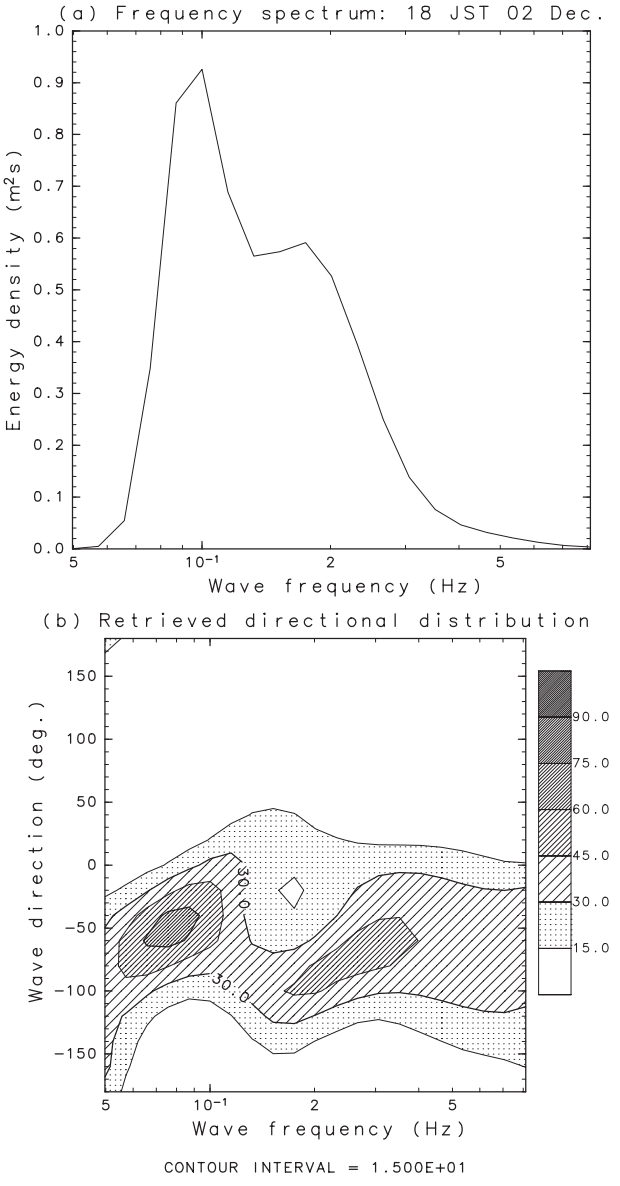

FIG. 6. Radar-estimated (a) frequency spectrum $E(f) = 2\pi \int_{-\pi}^{\pi} F(r, \theta_b, \omega, \theta)\, d\theta$ and (b) normalized directional distribution (%) $D(f, \theta) = 2\pi F(r, \theta_b, \omega, \theta)/E(f)$ at $(i_r, j_b) = (3, 4)$ at 1800 LST 2 Dec 2000.

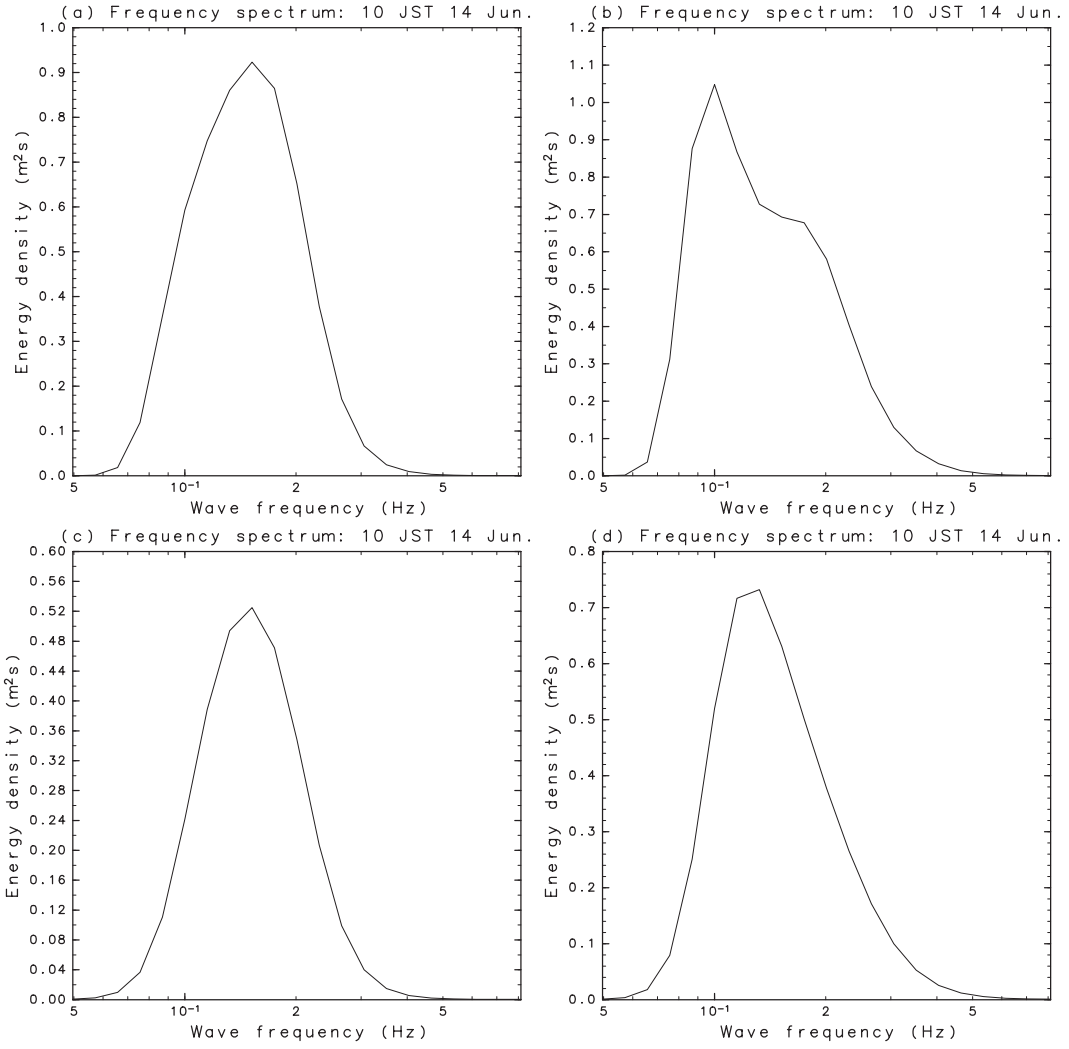

FIG. 7. Radar-estimated frequency spectra $E(f)$ at $(i_r, j_b) = (3, 4)$ at 1000 LST 14 Jun 2001 for cases (a) A-1, (b) C-1, (c) A-2, and (d) C-2.

were less than 6 dB in 2000. The SNRs of the Doppler spectra in 2001 were higher than those in 2000.

c. *Waves and winds*

Figure 5 shows time series of significant wave heights H_s and hourly averaged wind vectors during the HF radar observation period. The maximum wave height during the HF radar observation period in 2000 was 3.4 m at 0400 LST 11 November. The variation of wave height is not large (Fig. 5a). The mean wave height is 1.16 m and the standard deviation of H_s is 0.64 m in Fig. 5a.

The wind directions were southward or southwestward in 2000 (Fig. 5b). Northwestward winds were also observed, often associated with a passage of a storm. Winds typically change because of the passage of typhoons or atmospheric fronts. Typhoon Yagi passed in the south of the HF radar observation area on 25 October 2000. An atmospheric front passed over the HF radar observation area on 30 October 2000. Typhoon Xangsane passed to the west of the HF radar observation area on 1 November 2000.

The mean significant wave height during the HF radar observation period was only 0.53 m in 2001 (Fig. 5c). The maximum wave height was 1.65 m at 1600 LST 24 June, and the minimum wave height was 0.14 m at 1200 LST 9 June. The standard deviation was 0.32 m, which is smaller than the root-mean-square (rms) difference between in situ observations and radar-estimated significant wave heights H_r by 25-MHz radar (Hisaki 2005).

Northward winds were dominant in 2001 (Fig. 5d). In particular, most of the wind directions were northward after 4 June. No significant storms passed near the HF radar observation area in 2001. In the case of northwestward winds, the fetch is limited (Fig. 1).

TABLE 1. Rating of the comparison between HF ocean radar–derived wave heights H_r and USW significant wave heights H_s.

A	$1/1.1 \le H_r/H_s \le 1.1$, or $\lvert H_s - H_r \rvert \le 0.1$ (m)
B_+	$1.1 < H_r/H_s \le 1.3$, or $0.1 < H_r - H_s \le 0.15$ (m)
B_-	$1.1 < H_s/H_r \le 1.3$, or $0.1 < H_s - H_r \le 0.15$ (m)
C_+	$1.3 < H_r/H_s \le 1.5$, or $0.15 < H_r - H_s \le 0.25$ (m)
C_-	$1.3 < H_s/H_r \le 1.5$, or $0.15 < H_s - H_r \le 0.25$ (m)
D_+	$1.5 < H_r/H_s \le 1.7$, or $0.25 < H_r - H_s \le 0.35$ (m)
D_-	$1.5 < H_s/H_r \le 1.7$, or $0.25 < H_s - H_r \le 0.35$ (m)
E_+	$1.7 < H_r/H_s \le 1.9$, or $0.35 < H_r - H_s \le 0.45$ (m)
E_-	$1.7 < H_s/H_r \le 1.9$, or $0.35 < H_s - H_r \le 0.45$ (m)
F_+	$1.9 < H_r/H_s \le 2.1$, or $0.45 < H_r - H_s \le 0.55$ (m)
F_-	$1.9 < H_s/H_r \le 2.1$, or $0.45 < H_s - H_r \le 0.55$ (m)
G_+	$H_r/H_s > 2.1$, and $H_r - H_s > 0.55$ (m)
G_-	$H_s/H_r > 2.1$, and $H_s - H_r > 0.55$ (m)

5. Results

a. Examples of wave estimation

The wave spectra during the observation period were estimated at 16 grid points (Fig. 1), except when the HF radar system was stopped. Figure 6 shows an example of the wave spectrum at $(i_r, j_b) = (3, 4)$ estimated by HF radar. The weight parameters [λ_{wM} ($M = 1, \ldots, 6$) in Eq. (9)] are those for case A-1 (section 3b). Figure 6a shows the frequency spectrum $E(f)$, and Fig. 6b shows the normalized directional distribution $D(f, \theta) = 2\pi F(r, \theta_b, \omega, \theta)/E(f)$, where $f = \omega/(2\pi)$ is the wave frequency and θ is the counterclockwise direction with respect to the eastward direction. The significant wave height measured by USW is $H_s = 1.68$ m, and the radar-estimated wave height is $H_r = 1.45$ m. The wind direction was southward at the time, which is consistent with the directional distribution at higher frequencies.

Figure 7 shows examples of radar-estimated frequency spectra $E(f)$ at $(i_r, j_b) = (3, 4)$ for various cases (section 3b). The significant wave height by USW was $H_s = 1.56$ m. The frequency spectra were different for various cases. The radar-estimated wave heights were $H_r = 1.41$ m for case A-1 (Fig. 7a), $H_r = 1.49$ m for case C-1 (Fig. 7b), $H_r = 1.03$ m for case A-2 (Fig. 7c), and $H_r = 1.25$ m for case C-2 (Fig. 7d). The radar-estimated wave height is dependent on both the weights

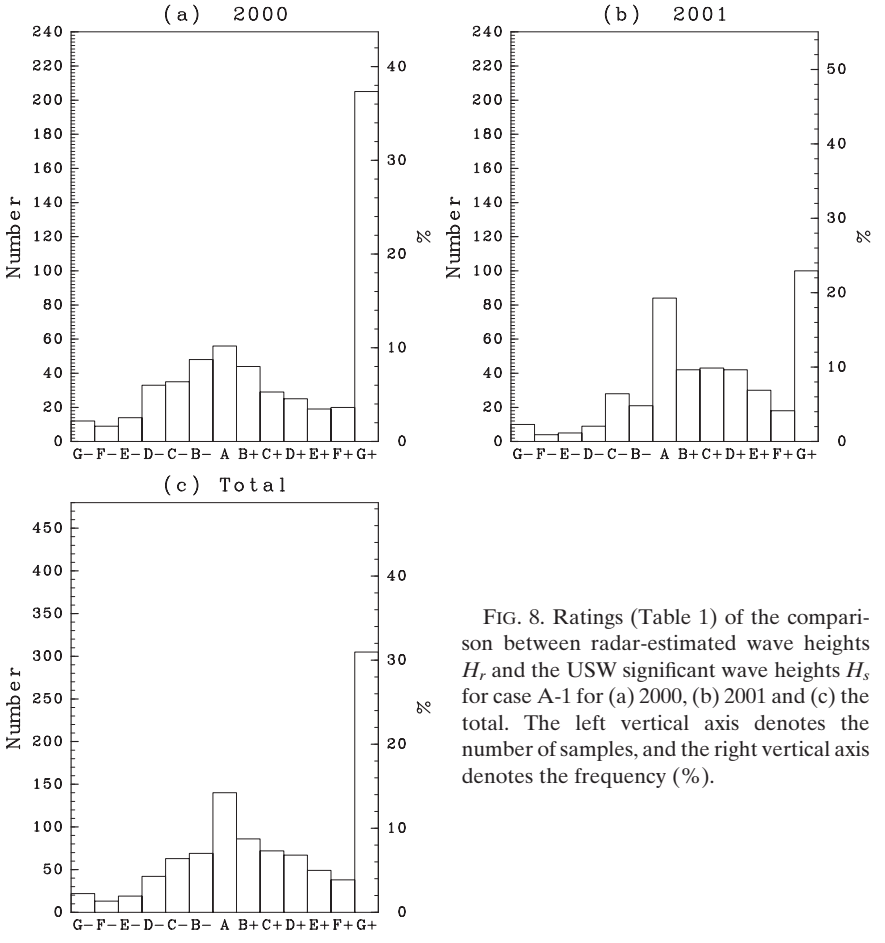

FIG. 8. Ratings (Table 1) of the comparison between radar-estimated wave heights H_r and the USW significant wave heights H_s for case A-1 for (a) 2000, (b) 2001 and (c) the total. The left vertical axis denotes the number of samples, and the right vertical axis denotes the frequency (%).

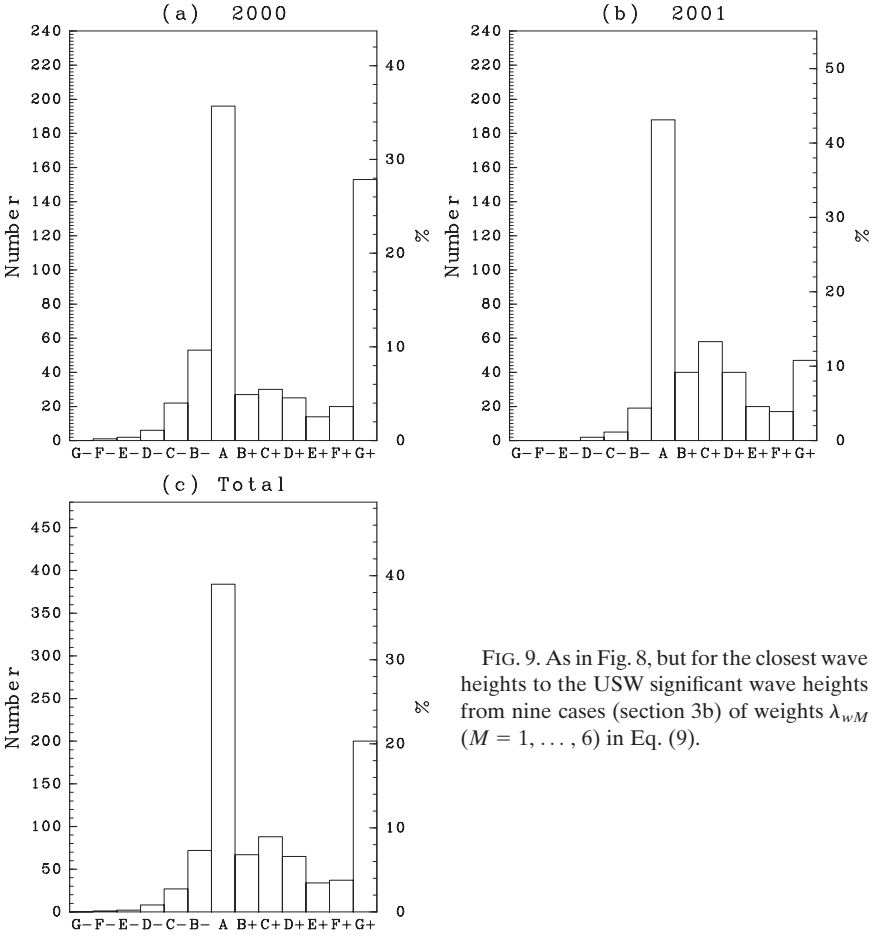

FIG. 9. As in Fig. 8, but for the closest wave heights to the USW significant wave heights from nine cases (section 3b) of weights λ_{wM} ($M = 1, \ldots, 6$) in Eq. (9).

λ_{wM} ($M = 1, \ldots, 6$) in Eq. (9) and the initial guess in the second step (section 2b).

We compared the radar-estimated wave heights H_r with USW significant wave heights H_s. The comparison is categorized from A to G_+ or G_-, as shown in Table 1. The subscript + denotes overestimation of radar wave heights H_r and subscript − denotes underestimation of radar wave heights H_r. Because the minimum USW wave height was less than 0.15 m (Fig. 5c), the rating of the comparison is based on either the ratio of wave heights (H_r/H_s) or their difference ($H_r - H_s$).

Figure 8 shows a comparison of the radar-estimated wave heights at $(i_r, j_b) = (3, 4)$ and the USW significant wave heights in case A-1. All of the radar-estimated wave heights are compared with H_s. The number of comparisons are 549 and 436 in 2000 and 2001, respectively. The rating G_+ was the most frequent, particularly in 2000. This means that Doppler spectra are often affected by spurious signals, and the SNRs of Doppler spectra are very low especially in 2000, as presented in section 4b. There are no correlations between H_r and H_s. The result that G_+ is the most frequent shows that excluding Doppler spectra of large R_{12} [Eq. (10)] values does not completely exclude the Doppler spectra affected by spurious signals. The second most frequent rating was A in both 2000 and 2001, which suggests that radar-estimated wave heights agree well with in situ observations if the Doppler spectra contaminated by spurious signals can be completely excluded.

The wave spectra are calculated for nine (3×3) cases, as in section 3b. The best wave heights, which are the closest to the USW significant wave heights H_s, are selected from nine wave heights H_r at each time. Figure 9 shows a comparison of the best wave heights and the USW significant wave heights. The most frequent rating was A in both 2000 and 2001. The rating G_+ was the second most frequent rating in 2000 and the third most frequent rating in 2001. If the radar-estimated wave data are selected properly from various cases in section 3b (various pairs of weights in the second and the third step), the waves can be estimated. However, there are radar-estimated wave data that should be eliminated in any case. The method to select radar-estimated wave data is described in section 3d.

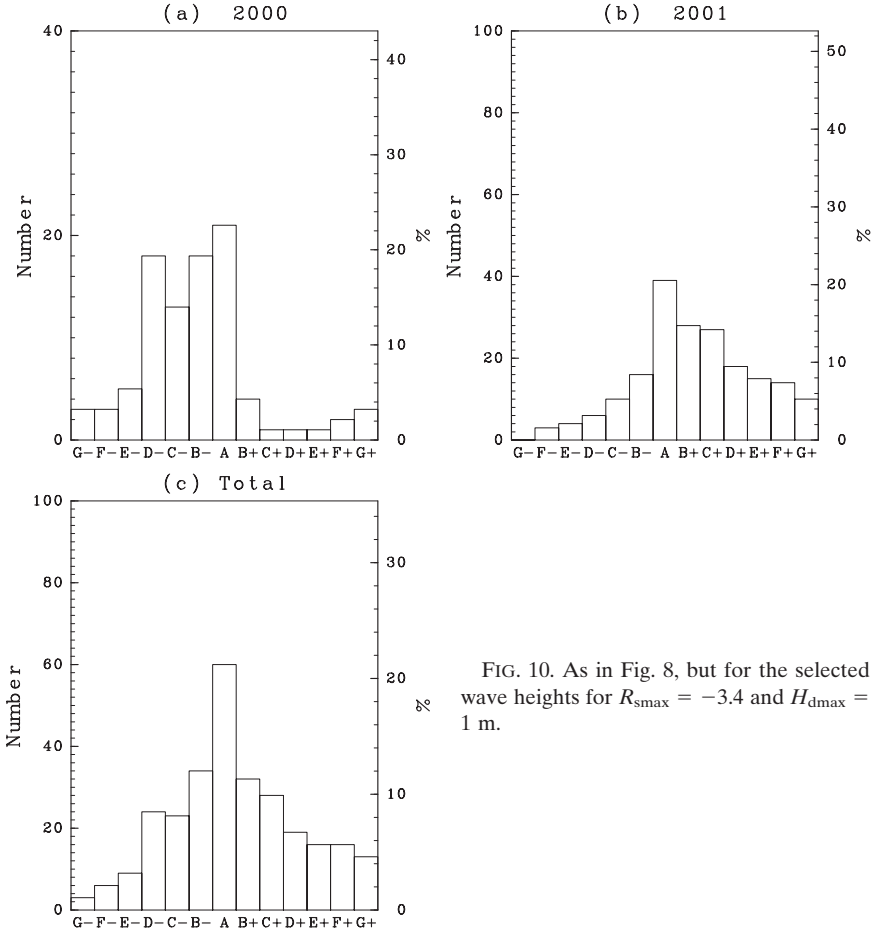

FIG. 10. As in Fig. 8, but for the selected wave heights for $R_{smax} = -3.4$ and $H_{dmax} = 1$ m.

b. Comparison of selected wave data

Figure 10 shows the comparison of selected radar wave heights (section 3d) and the USW significant wave heights for $R_{smax} = -3.4$ and $H_{dmax} = 1$ m. The number of wave data was 93 in 2000 and 190 in 2001. Although the total number of wave data in 2000 was larger than that in 2001, the total number of the selected wave data was smaller in 2000. This shows that most of the Doppler spectra in 2000 were significantly contaminated by noise. The frequency of the rating of G_+ becomes small by selecting wave data as in section 3d. The frequency of the rating A was the largest in both 2000 and 2001. The selected radar wave heights tended to be underestimated in 2000 and overestimated in 2001.

Figures 11a,b show the time series of selected radar-estimated wave heights H_r for $(R_{smax}, H_{dmax}) = (-3.4, 1$ m) and the USW significant wave heights H_s in 2000 and 2001, respectively. The radar-estimated wave heights H_r were underestimated in 2000, especially from 10 to 15 November, and overestimated in 2001. In particular, from 8 to 10 June and 26 June 2001, when the USW significant wave heights were low (less than 0.5 m), radar-estimated wave heights H_r were often overestimated.

Figure 11c is the scatterplot between USW significant wave heights H_s and selected radar wave heights H_r for $(R_{smax}, H_{dmax}) = (-3.4, 1$ m). The rms difference between H_s and H_r was $\Delta_{rms} = 0.38$ m, and the correlation coefficient was $r_c = 0.73$, where the number of samples is 283. The mean USW significant wave height for the comparison was 0.83 m and the standard deviation of the USW significant wave heights was 0.55 m. Although the mean and standard deviation of wave heights were small, the radar-estimated wave heights correlated with in situ observations.

Figures 12a–e show the rms differences, correlation coefficients, mean USW significant wave height for the comparison, standard deviation of the USW significant wave heights, and ratio of the selection for various H_{dmax} and R_{smax}, as discussed in section 3d. The selection ratio (Fig. 12e) became smaller for smaller H_{dmax} and R_{smax} values, which is obvious from the definition of H_{dmax} and R_{smax}. The rms difference (Fig. 12a) was smaller for larger H_{dmax} and smaller R_{smax}. However, the decrease of the

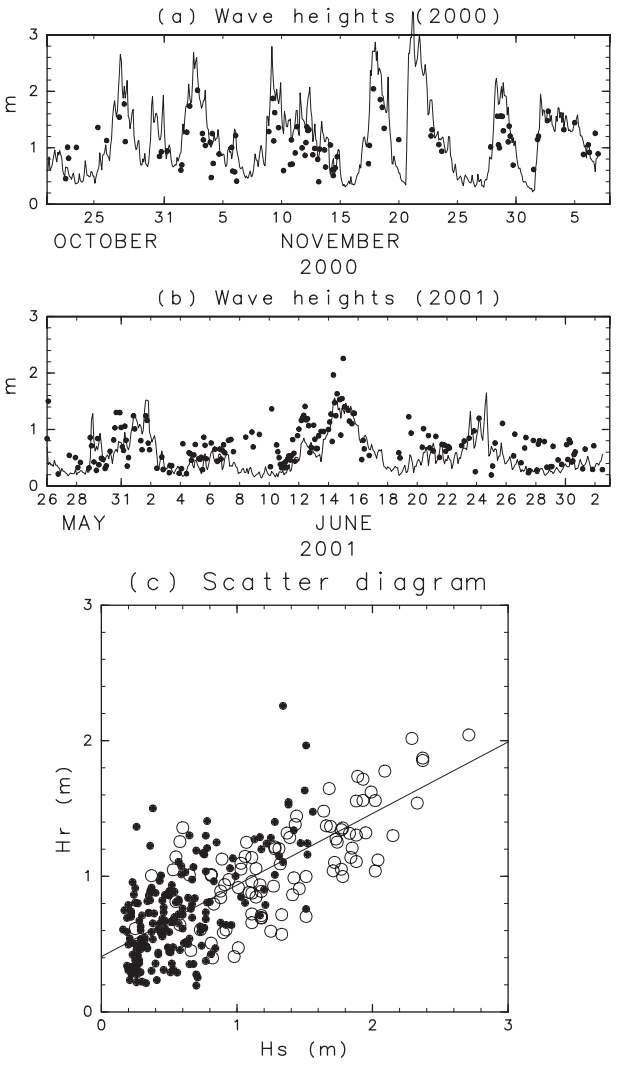

FIG. 11. Comparison of selected radar-estimated wave heights H_r for (R_{smax}, H_{dmax}) = (−3.4, 1 m) and USW significant wave heights H_s. Time series in (a) 2000 and (b) 2001 (solid line: H_s, dots: H_r). (c) Scatterplot between H_s and H_r [white circle: 2000, black circle: 2001].

rms difference with larger H_{dmax} was not clear for $H_{\mathrm{dmax}} >$ 1 m in Fig. 12a. Figure 12b shows the contour map of $100(r_c - 0.7)$. For example, the contour value of 2 denotes that the correlation coefficient is $r_c = 0.72$. The correlation coefficient between H_s and H_r is about 0.7 in this case. The correlation coefficient is larger for smaller R_{smax} values. On the other hand, the correlation coefficient was the largest at $H_{\mathrm{dmax}} \simeq 1$ m, which shows the optimal value of H_{dmax} for radar-estimated wave selection. The mean value of the USW significant wave height for the comparison was higher for larger R_{smax} values and larger H_{dmax} values when $H_{\mathrm{dmax}} > 1$ m (Fig. 12c). The standard deviation of the USW significant wave height for the comparison was also higher for larger R_{smax}. The smaller the standard deviation, the smaller the correlation is expected to be, but the correlation is larger for smaller R_{smax} (Fig. 12b), which shows that the residual of the second-order radar equation [Eq. (7)] is an adequate parameter for selecting radar-estimated wave data.

Figure 12f shows the frequency that $|H_s(t + \Delta t) - H_s(t)| > H_{\mathrm{dmax}}$ for various H_{dmax} values estimated by total USW significant wave heights from 1997 to 2001. The time interval of USW significant wave heights is $\Delta t = 2$ h, and the total number of $|H_s(t + \Delta t) - H_s(t)|$ is 16 612, which is smaller than 21 912 because of the missing data. The frequency at which $|H_s(t + \Delta t) - H_s(t)| > H_{\mathrm{dmax}}$ was 2.63%, 0.30%, and 0.078% for $H_{\mathrm{dmax}} =$ 0.5 m, $H_{\mathrm{dmax}} = 1$ m, and $H_{\mathrm{dmax}} = 1.5$ m, respectively. The possibility that the wave height changes more than 1 m is very rare.

6. Discussion and conclusions

The wave spectrum estimated from HF radar is very sensitive to the noise of the Doppler spectrum. The present method can estimate even when a few second-order Doppler spectra are missing. In estimating wave spectra, it is critical to exclude the Doppler spectra that are significantly contaminated by spurious signals. The method based on the second-order Doppler spectral peak levels with respect to the noise floor is not suitable for selecting Doppler spectra to estimate ocean wave spectra, because if the wave height is low, the peak levels are low. The Doppler spectra with spurious signals cannot be removed in this method.

The method from the value of R_{12} [Eq. (10)] was attempted to exclude the contaminated Doppler spectra. Then, Doppler spectra were spatially averaged to reduce the number of unknowns (i.e., N_u). The noise floor, which is evaluated by the rank ordering technique (Heron and Heron 2001), was subtracted from the Doppler spectra. Some contaminated Doppler spectra may have been excluded by the method using the value of R_{12}, but the method overall proved insufficient. Some radar-estimated wave heights were significantly overestimated compared with USW significant wave heights. The radar-estimated wave data should be selected or eliminated.

The present method to estimate wave spectra was converted to a nonlinear optimizing problem. The solution is dependent on the initial guess of the iterative algorithm. The solution is also dependent on the weights λ_{wM} ($M = 1, \ldots, 6$) in Eq. (9). The radar-estimated wave data are selected based on the residuals of the second-order radar cross-sectional equation [Eq. (7)] and the energy balance equation. The significantly overestimated radar wave heights can be removed. The correlation

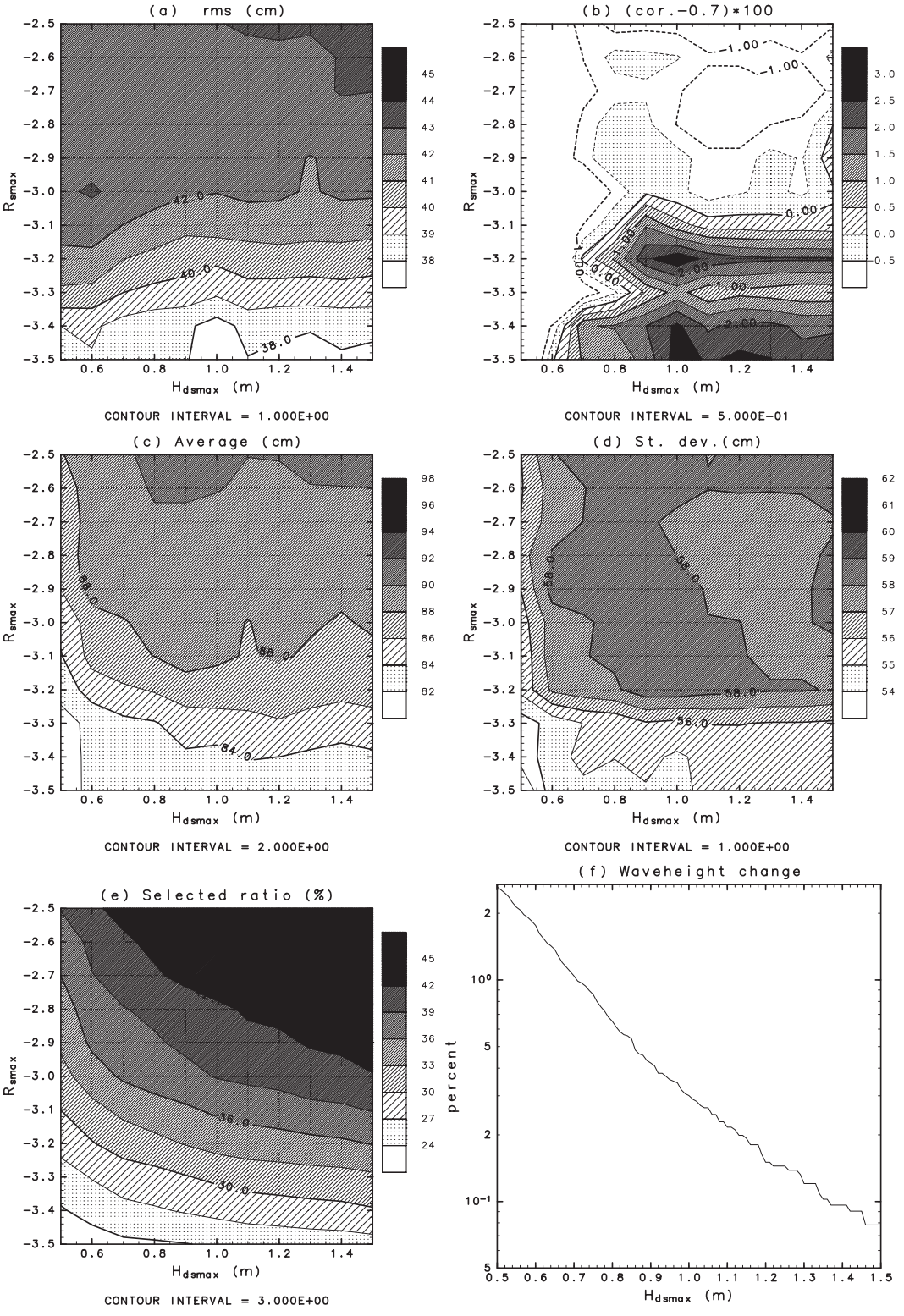

FIG. 12. (a) The rms difference (cm) between selected radar-estimated wave heights H_r and USW significant wave heights H_s as a function of H_{dmax} and R_{smax}. (b) As in (a), but $100(r_c - 0.7)$, where r_c is the correlation coefficient of H_r and H_s. (c) Mean USW significant wave heights (cm) for the comparison, (d) standard deviation (cm) of the USW significant wave heights for the comparison, and (e) ratio (%) of the selection (section 3d). (f) Frequency (%) at which $|H_s(t + \Delta t) - H_s(t)| > H_{\mathrm{dmax}}$ for various H_{dmax}.

between radar-estimated wave heights and in situ observations is good, considering the low-SNR Doppler spectra and small temporal variability of wave heights.

The wind speeds are also estimated; however, there was no correlation between radar-estimated wind speeds and observed wind speeds at the land-based wind station, whereas there was such a correlation in Hisaki (2005). The wind speeds are decided from initial wind speeds estimated from the high-frequency spectral values in the second step (section 2b). High-frequency spectral values cannot be exactly estimated in the case of $\Phi(\sigma) = \sigma$ [Eq. (7)], because the estimated wave spectrum is insensitive to smaller values of $P_{c2}(\omega_D)$. On the other hand, $\Phi(\sigma) = \log(\sigma)$ in Hisaki (2005) and high-frequency spectral values could be estimated. A method to estimate wind speeds from the wind wave spectrum should be explored.

The optimal values of criteria H_{dmax} and R_{smax} are decided from the correlation (Fig. 12a), rms difference (Fig. 12b), selection ratio (Fig. 12e) and frequency of wave height change (Fig. 12f). For example, if the required accuracy of wave heights is less than 0.4 m, the criterion R_{smax} should be less than -3.3. In any requirement of accuracy, it is recommended that $H_{\mathrm{dmax}} > 0.9$ m.

The wave heights and SN ratios of Doppler spectra were low during the HF radar observation period. We can expect that the SN ratios of Doppler spectra would be higher if wave heights were higher, and the selection ratio of wave data would be increased. On the other hand, two factors can affect the wave estimation by HF radar. One factor is that the sea state affects the ground wave loss for propagating HF radio waves across the ocean (Barrick 1971b). The signals of Doppler spectrum become lower as the wave height becomes higher. The other factor is the breakdown of the second-order scattering theory [Eq. (A2)], if the wave height H_s is larger than $2/k_0$ (Lipa and Barrick 1986). The selection ratio of wave data will be increased at higher wave height, but there is a limit to the increase.

Although the minimum number of second-order Doppler spectra or minimum K_{DT} for estimating wave spectra is unclear, it is unnecessary to investigate the minimum number or K_{DT}. If the number of constraints is larger than number of unknowns, (i.e., $N_t \geq N_u$), the solution can be estimated. We selected or eliminated the solution by the method proposed in this study. To increase the selection ratio (Fig. 12e), a method to select or eliminate the Doppler spectra should be developed.

Acknowledgments. The author acknowledges the anonymous reviewers for their insightful comments, which contributed to the improvement of the manuscript. This study was financially supported by a Grant-in-Aid for Scientific Research (C-2) from the Ministry of Education, Culture, Sports, Science, and Technology of Japan (20540429). The author acknowledges the Okinawa Radio Observatory, Communications Research Laboratory (Okinawa Subtropical Environment Remote-Sensing Center, National Institute of Information and Communications Technology) for providing Doppler spectrum data from HF ocean radar and the Japan Meteorological Agency for providing meteorological data. The wave data were supplied by the Coastal Development Institute of Technology. The GFD-DENNOU Library (available online at http://dennou.gaia.h.kyoto-u.ac.jp/arch/dcl/) was used for drawing the figures.

APPENDIX A

Equations to Estimate Wave Spectra

The equations to estimate wave spectra are as follows: the first- and second-order radar cross sections are

$$\sigma_1(\omega_D) = 2^6 \pi k_0^4 \sum_{m=\pm 1} S(-2m\mathbf{k}_0)\delta(\omega_D - m\omega_B) \quad \text{and} \tag{A1}$$

$$\sigma_2(\omega_D) = 2^6 \pi k_0^4 \sum_{m_1=\pm 1} \sum_{m_2=\pm 1} \int_{-\infty}^{+\infty} \int_{-\infty}^{+\infty} |\Gamma_E^s \cdot - i\Gamma_H^s|^2 \times S(m_1\mathbf{k}_1) S(m_2\mathbf{k}_2) \delta[\omega_D - m_1(gk_{d1})^{1/2} - m_2(gk_{d2})^{1/2}]\, d\boldsymbol{\kappa}, \tag{A2}$$

respectively, where $S(\mathbf{k}) = F(\omega, \theta)C_g/k$ is the wave spectrum in terms of wavenumber vector $\mathbf{k} = (k\cos\theta, k\sin\theta)$, $\mathbf{k}_0$ is the incident radio wavenumber vector, and δ is Dirac's delta function. The integral variable $\boldsymbol{\kappa}$ in Eq. (A2) is the two-dimensional vector, and the vector $\mathbf{k}_m$ ($m = 1, 2$) is $\mathbf{k}_m = -\mathbf{k}_0 + (3 - 2m)\boldsymbol{\kappa}$. The variable $k_{dm} = |\mathbf{k}_{dm}|$ ($m = 1, 2$) in Eq. (A2) is $\mathbf{k}_{dm} = \tanh(k_m d)\mathbf{k}_m$, where $k_m = |\mathbf{k}_m|$ ($m = 1, 2$) and d is the water depth.

The coefficients in Eq. (A2) are

$$\Gamma_H^s = \frac{1}{2}\left\{ k_{d1} + k_{d2} + \frac{(k_{d1}k_{d2} - \mathbf{k}_{d1}\cdot\mathbf{k}_{d2})}{m_1 m_2 (k_{d1}k_{d2})^{1/2}} \left(\frac{\omega_B^2 + \omega_D^2}{\omega_B^2 - \omega_D^2}\right) + \frac{\omega_D[m_1 k_{d1}^{3/2}\,\mathrm{cosech}^2(k_1 d) + m_2 k_{d2}^{3/2}\,\mathrm{cosech}^2(k_2 d)]}{g(\omega_D^2 - \omega_B^2)} \right\}, \tag{A3}$$

and

$$\Gamma_E^s = \frac{1}{2}\left[\frac{(\mathbf{k}_1 \cdot \mathbf{k}_0)(\mathbf{k}_2 \cdot \mathbf{k}_0)/k_0^2 - 2\mathbf{k}_1 \cdot \mathbf{k}_2}{(\mathbf{k}_1 \cdot \mathbf{k}_2)^{1/2} - k_0\Delta}\right], \quad \text{(A4)}$$

where Δ is the normalized surface impedance, and $\Delta = 0.011 - 0.012i$ (Lipa and Barrick 1986). The energy balance equation (constraint 3 in section 2a) is

$$\mathbf{C}_g \cdot \nabla F(\omega, \theta) - S_t = 0, \quad \text{(A5)}$$

where $\mathbf{C}_g$ is a group velocity vector, S_t is the source function, and ∇ denotes the horizontal gradient. The continuity equation of winds (constraint 4 in section 2a) is

$$\nabla \cdot \mathbf{u}_w = 0, \quad \text{(A6)}$$

where $\mathbf{u}_w$ represents the sea surface wind vectors. Constraint 5 in section 2a is expressed as

$$\log[F(k_f+1, l_d)] + \log[F(k_f-1, l_d)] + \log[F(k_f, l_d-1)] + \log[F(k_f, l_d+1)] - 4\log[F(k_f, l_d)] = 0$$
$$\text{for} \quad 1 < k_f < M_f \quad \text{or} \quad \log[F(k_f, l_d-1)] + \log[F(k_f, l_d+1)] - 2\log[F(k_f, l_d)] = 0, \quad \text{for} \quad k_f = 1, M_f, \quad \text{(A7)}$$

where $F(k_f, l_d) = F(k_f, l_d, i_r, j_b)$ is the wave directional spectrum for frequency number k_f, direction number l_d, range index number i_r, and beam index number j_b. Constraint 6 in section 2a is

$$\mathbf{C}_g \cdot \nabla F(\omega, \theta) = 0. \quad \text{(A8)}$$

APPENDIX B

Equations for the Algorithm

The parametric form for the initial guess of the wave spectrum in the first step (section 2b) is

$$F(\omega, \theta) = \frac{1}{2\pi} E(f) D(f, \theta), \quad \text{(B1)}$$

$$E(f) = \frac{\alpha g^2}{2\pi}\omega^{-p} \exp\left[-\frac{p}{p-1}\left(\frac{f}{f_p}\right)^{1-p}\right], \quad \text{and} \quad \text{(B2)}$$

$$D(f, \theta) = D[f(k_f), \theta] = \cos^{2s}\left[\frac{\theta - \theta_a(k_f)}{2}\right]\left[\int_{-\pi}^{\pi} \cos^{2s}\left(\frac{\theta}{2}\right) d\theta\right]^{-1}, \quad \text{(B3)}$$

where $E(f)$ is the frequency spectrum at the frequency $f = \omega/(2\pi)$, $D(f, \theta)$ is the directional distribution, and $\theta_a(k_f)$ is the mean wave direction for frequency number k_f. The parameter $\theta_a(k_f)$ was set as

$$\theta_a(k_f) = \theta_w + [2r_q(k_f) - 1]\Delta\theta_{\text{bd}}, \quad \text{for} \quad k_f \geq k_B \quad \text{and} \quad \text{(B4)}$$

$$\theta_a(k_f) = \theta_a(k_f + 1) + [2r_q(k_f) - 1]\Delta\theta_{\text{nd}}, \quad \text{for} \quad k_f < k_B, \quad \text{(B5)}$$

where θ_w is the initial guess for wind direction estimated from the ratio of first-order scattering; k_B is the frequency number, so that $f = f(k_B)$ is close to $f_B = \omega_B/(2\pi)$; and $r_q(k_f)$ ($k_f = 1, \ldots, M_f$) are the random numbers of $0 \leq r_q(k_f) \leq 1$, $\Delta\theta_{\text{bd}} = 15°$, and $\Delta\theta_{\text{nd}} = 10°$. The parameters α, f_p, p, s, and $r_q(k_f)$ ($k_f = 1, \ldots, M_f$) are unknowns to be estimated from the ranges decided upon in the first step of section 2b.

The iterative algorithm is expressed as follows:

$$\mathbf{d}_m = -\mathbf{H}^{(m)}\mathbf{J}_f^{\mathrm{T}}\mathbf{f} \quad \text{and} \quad \text{(B6)}$$

$$\mathbf{x}^{(m+1)} = \mathbf{x}^{(m)} + \alpha_m \mathbf{d}_m, \quad \text{(B7)}$$

where m indicates the step number and α_m is a positive constant that has been adjusted such that $U[\mathbf{x}^{(m+1)}] < U[\mathbf{x}^{(m)}]$. The vector $\mathbf{x}^{(m)} = [x_1^{(m)}, \ldots, x_{N_u}^{(m)}]$ is $\mathbf{x}$ for the mth step. The vector $\mathbf{f} = (f_K) = (\lambda_{wM} F_K)$ ($K = 1, \ldots, N_t$), and $\mathbf{J}_{\text{f}}$ is the Jacobian matrix defined as

$$\mathbf{J}_{\text{f}}(K, L) = \frac{\partial f_K}{\partial x_L^{(m)}} \quad (K = 1, \ldots, N_t) \quad (L = 1, \ldots, N_u). \quad \text{(B8)}$$

The positive definite matrix $\mathbf{H}^{(m)}$ is set as

$$\mathbf{H}^{(m)} = [\text{diag}(\mathbf{J}_{\text{f}}^{\mathrm{T}}\mathbf{J}_{\text{f}})]^{-1}, \quad \text{(B9)}$$

$$\mathbf{H}^{(m)} = [\text{diag}(\mathbf{J}_{\text{f}}^{\mathrm{T}}\mathbf{J}_{\text{f}}) + \mathbf{I}]^{-1}, \quad \text{(B10)}$$

or $\mathbf{H}^{(m)} = \mathbf{I}$, where diag() denotes the diagonal matrix for the square matrix and $\mathbf{I}$ is the unit matrix.

REFERENCES

Barrick, D. E., 1971a: Dependence of second-order sidebands in HF sea echo upon sea state. *Proc. Antennas and Propagation Society Int. Symp.,* Los Angeles, CA, IEEE, 194–197.

——, 1971b: Theory of HF/VHF propagation across the rough sea, 2, Application to HF/VHF propagation above the sea. *Radio Sci.,* **6,** 527–533.

——, 1977: The ocean wave height nondirectional spectrum from inversion of the HF sea-echo Doppler spectrum. *Remote Sens. Environ.,* **6,** 201–227.

Cochin, V., V. Mariette, P. Broche, and R. Garelloand, 2006: Tidal current measurements using VHF Radar and ADCP in the Normand Breton Gulf: Comparison of observations and numerical model. *IEEE J. Oceanic Eng.,* **32,** 885–893.

Hashimoto, N., L. R. Wyatt, and S. Kojima, 2003: Verification of a Bayesian method for estimating directional spectra from HF radar surface backscatter. *Coastal Eng. J.,* **45,** 255–274.

Heron, M. L., and S. F. Heron, 2001: Cumulative probability noise analysis in geophysical spectral records. *Int. J. Remote Sens.,* **22,** 2537–2544.

Hisaki, Y., 1996: Nonlinear inversion of the integral equation to estimate ocean wave spectra from HF radar. *Radio Sci.,* **31,** 25–39.

——, 2002: Short-wave directional properties in the vicinity of atmospheric and oceanic fronts. *J. Geophys. Res.,* **107,** 3188, doi:10.1029/2001JC000912.

——, 2005: Ocean wave directional spectra estimation from an HF ocean radar with a single antenna array: Observation. *J. Geophys. Res.,* **110,** C11004, doi:10.1029/2005JC002881.

——, 2006a: Ocean wave directional spectra estimation from an HF ocean radar with a single antenna array: Methodology. *J. Atmos. Oceanic Technol.,* **23,** 268–286.

——, 2006b: Analysis of decomposed surface currents in a limited area. *IEEE J. Oceanic Eng.,* **32,** 768–778.

——, 2007: Directional distribution of the short-wave estimated from HF ocean radars. *J. Geophys. Res.,* **112,** C10014, doi:10.1029/2007JC004296.

——, and T. Naruke, 2003: Horizontal variability of near-inertial oscillations associated with the passage of a typhoon. *J. Geophys. Res.,* **108,** 3382, doi:10.1029/2002JC001683.

——, W. Fujiie, T. Tokeshi, K. Sato, and S. Fujii, 2001: Surface current variability east of Okinawa Island obtained from remotely sensed and in situ observational data. *J. Geophys. Res.,* **106,** 31 057–31 073.

Kohut, J. T., H. J. Roarty, and S. M. Glenn, 2006: Characterizing observed environmental variability with HF Doppler radar surface current mappers and acoustic Doppler current profilers: Environmental variability in the coastal ocean. *IEEE J. Oceanic Eng.,* **32,** 876–884.

Lipa, B. J., and D. E. Barrick, 1986: Extraction of sea state from HF radar sea echo: Mathematical theory and modeling. *Radio Sci.,* **1,** 81–100.

——, and B. Nyden, 2005: Directional wave information from the SeaSonde. *IEEE J. Oceanic Eng.,* **30,** 221–231.

Paduan, J. D., K. C. Kim, M. S. Cook, and F. P. Chavez, 2006: Calibration and validation of direction-finding high-frequency radar ocean surface current observations. *IEEE J. Oceanic Eng.,* **31,** 862–875.

WAMDI Group, 1988: The WAM model—A third generation ocean wave prediction model. *J. Phys. Oceanogr.,* **18,** 1775–1810.

Wyatt, L. R., and Coauthors, 2003: Validation and intercomparisons of wave measurements and models during the EuroROSE experiments. *Coastal Eng.,* **48,** 1–28.